Strong enhancement of surface diffusion by nonlinear surface acoustic waves

Maxim V. Shugaev,[1] Anthony J. Manzo,[2] Chengping Wu,[1] Vladimir Yu. Zaitsev,[1,3,4]
Henry Helvajian,[2] and Leonid V. Zhigilei[1,*]

[1]*Department of Materials Science and Engineering, University of Virginia, 395 McCormik Road, Charlottesville, Virginia 22904-4745, USA*
[2]*Physical Sciences Laboratories, The Aerospace Corporation, P.O. Box 92957, Los Angeles, California 90009-2957, USA*
[3]*Institute of Applied Physics, Russian Academy of Sciences, Uljanova St. 46, Nizhny Novgorod, 603950, Russia*
[4]*Nizhny Novgorod State University, Gagarina Avenue 23, Nizhny Novgorod, 603950, Russia*

The phenomenon of acoustic activation of surface diffusion is investigated in a combined computational and experimental study. The ability of pulsed laser-generated surface acoustic waves (SAWs) to enhance the mobility of small atomic clusters is demonstrated by directly tracking, with fluorescence microscopy, individual Au_8 clusters moving on a (111) silicon substrate. A 19-fold increase in the effective diffusion coefficient is measured in room temperature experiments in the presence of SAWs generated by nanosecond pulse laser irradiation at a 100 Hz repetition rate. A strong enhancement of cluster mobility by SAWs is also observed in large-scale molecular dynamics simulations of surface diffusion of small atomic clusters. The analysis of the computational results demonstrates that the nonlinear sharpening of SAWs and the corresponding enrichment of the SAW spectra by high frequency harmonics which are capable of dynamic coupling to the cluster vibrations are responsible for the efficient acoustic activation of surface mobility in the simulations. The increase in the effective diffusion coefficient is proportional to the number of the SAW pulses passing through the diffusion region per unit time and a dramatic 4500-fold diffusion enhancement (corresponds to an equivalent temperature increase by $\sim 10^3$ K) is predicted in the simulations for 15 GHz SAWs. The ability of SAWs to affect atomic-level surface processes has far-reaching implications for the design of new techniques where the acoustic energy serves as an effective substitution for thermal activation in applications where heating must be avoided or rapid switching of surface conditions is required.

I. INTRODUCTION

Surface acoustic waves (SAWs) are actively used in many practical applications, including signal processing [1], chemical sensing [2,3], nondestructive evaluation of mechanical properties [4,5], and microscale manipulation of fluid flow in microfluidics devices [6,7]. Moreover, there is growing experimental evidence of the ability of SAWs to affect surface processes at the atomic/molecular level. In particular, SAWs and bulk acoustic waves interacting with surfaces have been shown to be able to substantially enhance the rates and selectivity of heterogeneous catalytic reactions [8–16], desorb molecules, atoms, and ions from surfaces [13,17–23], and facilitate surface diffusion of small atomic clusters [24]. These observations are surprising as there is a large mismatch between the relatively low frequencies of the acoustic waves, typically less than 100 MHz, and the vibrational frequencies characteristic of atoms and molecules on the surface, on the order of terahertz. This frequency mismatch calls into question the contribution of the dynamic resonant coupling of the acoustic wave to surface vibrational states [19,21,25,26] and gives rise to hypotheses based on the presumed presence of mesoscopic-scale substructures/domains [10,12] that can effectively couple to a long-wavelength acoustic excitation, nanoscale stressed surface features that can release the stored strain energy in response to an acoustic activation, thus providing the needed extra energy for the desorption of molecules [22], or acoustically induced variation of the spatial distribution of adsorbates to affect the surface reaction rates [15].

Modification of the binding energies and diffusion barriers of adsorbed species induced by the surface strain [27–33] has also been considered as a mechanism responsible for the acoustic activation of surface processes [16,34]. Indeed, a recent theoretical and computational analysis performed for linear (sinusoidal) elastic SAWs [35] suggests that a combined effect of the transient modification of the diffusion barriers and adiabatic temperature variation due to the periodic oscillations of the acoustic strain can lead to a noticeable enhancement of surface diffusion for large strain magnitudes and systems that exhibit strong strain dependence of the diffusion barriers [27–33]. The large surface strains ($\sim 10^{-2}$) required for reaching practically relevant levels of the diffusion enhancement and the strong quadratic scaling of the diffusion enhancement with the strain amplitude in the absence of nonlinear enrichment of SAW spectrum by higher harmonics [35], however, make the assumption of the linear SAW propagation questionable and suggest that nonlinear effects should be considered.

In this paper, we report the results of a combined computational and experimental study targeted at resolving the longstanding question on the mechanism of the acoustic activation of surface processes. A simple model system consisting of small atomic clusters moving on a substrate exposed to SAWs is considered in both simulations and experiments. The experimental results provide direct evidence of strong acoustic enhancement of surface mobility of atomic clusters. The simulations also predict a dramatic diffusion enhancement by SAWs and link it to the nonlinear wave profile sharpening accompanied by the generation of high frequency harmonics that effectively couple to the vibrational modes of the clusters. The mechanistic insights into the key role of the nonlinear effects in the SAW-induced activation of surface

*lz2n@virginia.edu

processes provide guidelines for the design and optimization of a new class of applications in the areas of chemical catalysis, low temperature thin film growth, and mass spectrometry of heat sensitive molecules.

II. EXPERIMENTAL METHOD

The schematic of the experimental setup designed for the investigation of the effect of SAWs on surface mobility of small atomic clusters is shown in Fig. 1. It comprises a high magnification ($100\times$, 0.90 numerical aperture, through-air objective) imaging microscope with an electron multiplying charge coupled device (EMCCD) camera for low light level detection, a 100 Hz repetition rate 6 ns pulse laser configured to generate two wavelengths (355 and 532 nm) simultaneously, a wafer-substrate holder mounted on top of a nanometer precision piezo-driven XY stage, spatial and spectral filters, optics for controlled metering of the laser power, and a computer that gathers image data from the EMCCD and synchronizes the experiment. The whole apparatus is mounted on a vibration isolation table housed in a class 10000 clean room that is temperature controlled to $\pm 1.1\,^{\circ}$C.

A. Sample preparation and imaging

The experiments are performed for monodispersed Au_8 clusters prepared on crystalline (111) silicon substrate (with native oxide). The candidate cluster chosen is gold because it is sufficiently inert on native oxide and is used in numerous applications (e.g., optoelectronics, biorecognition, catalyst immobilization, and catalysis). The experiments are conducted in air, at room temperature, and utilize a molecular tracking technique used in super resolution imaging microscopy [36–39]. Monodispersed Au_8 clusters with a surface density range of $\sim 3-9 \times 10^{-2}\,\mu m^{-2}$ are generated directly on the silicon substrate by 532 nm pulsed laser ablation of 15 nm gold nanoparticles using the plasmon absorption band [40]. The Au_8 species are identified and tracked using high magnification imaging and well known fluorescence signatures of Au_n [41–44].

B. Generation of SAWs

A pulsed Nd:YAG laser operating at 355 nm wavelength, 6 ns pulse duration, and 100 Hz repetition rate is used for the generation of SAWs, in lieu of a traditional piezoelectric transducer. In addition to being a nonmechanical contact scheme, the optical generation of SAWs also provides the flexibility of controlling the wave packet bandwidth by adjusting the laser focal spot size and pulse width [45,46]. The SAWs with plane fronts are generated by focusing laser pulses with a cylindrical lens (10 cm focal length) to form a rectangular spot with 5 mm length and $12-20\,\mu m$ width ($16\,\mu m$ on average). The propagating plane fronts are not aligned with any particular crystallographic direction in the silicon substrate. Furthermore, of the two counter propagating plane fronts, the "forward" is directed toward the observation zone while the "backward" travelling wave is directed away by using an oblique edge in the cut silicon substrate. An incident laser fluence of 0.75 J/cm^2 is chosen to be close but still below the ablation threshold (for single shot excitation), so that strong SAW pulses can be generated by repeated irradiation at the same location. Note that further enhancement of SAWs by adding a sacrificial ablating layer (e.g., a liquid suspension of carbon particles [4,5,47]) cannot be applied in this study since the ablation debris field would disturb the image data acquisition. Consequently, the generation of strong SAWs is achieved by applying the maximum laser fluence possible that still allows for nonablative multipulse irradiation of the substrate and ensures a high degree of localization of the initial
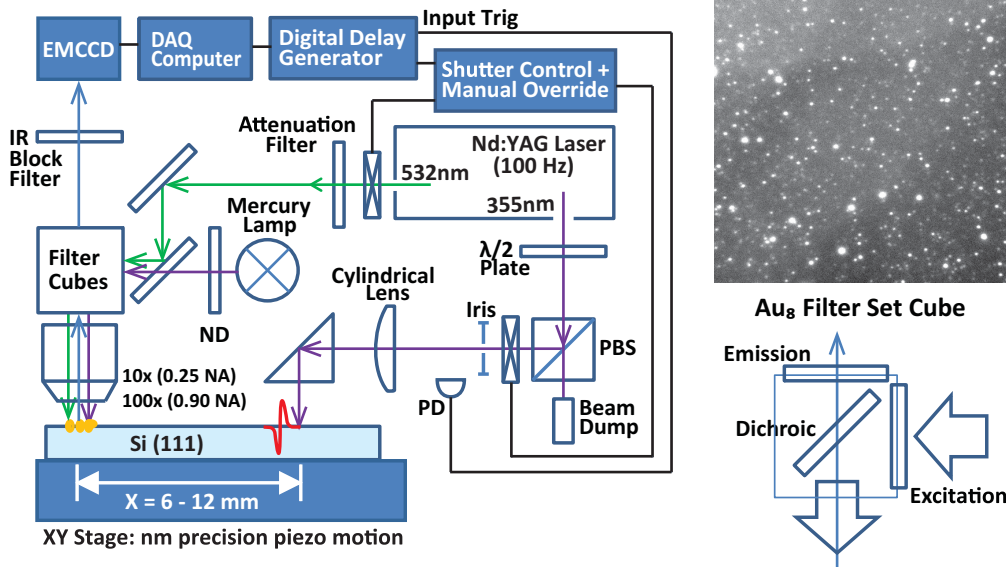

FIG. 1. (Color online) A schematic of the experimental setup (left), a processed image covering an area of 65.5 μm $\times$ 65.5 μm that shows a "debris" field of Au_8 species (upper right), and a schematic of the filter-cube with three filter combination used to spectrally resolve Au_8 (lower right). Time synchronization is initiated by a photodiode. The acronyms have the following meaning: PD – photodiode, EMCCD – electron multiplying charge coupled device, DAQ – data acquisition, IR – infrared, Trig – trigger, PBS – polarizing beam splitter, NA – numerical aperture, and ND - neutral density filter.

laser energy deposition near the surface (the optical absorption depth at a wavelength of 355 nm is about 9 nm [48], and the absorbed energy is redistributed by heat diffusion within the depth of $0.5-1\,\mu$m during the laser pulse).

C. Quantifying the mobility of Au$_8$ clusters

A statistically consistent data set for cluster mobility is assembled through a succession of process steps that starts by identifying an ensemble of clusters that are then followed by measuring individual displacements after a time interval. Details of this analysis are discussed in the Supplemental Material [49]. Consequently, we only provide a brief overview of our approach below. Following sample preparation and characterization, a 355 nm pulsed laser irradiates the sample to generate planar SAWs $6-12$ mm from the imaged region. The laser is periodically blocked to allow capture of a sequence of "cluster-field" images of the fluorescent Au$_8$. The image fields are then analyzed to define particle locations. In the case when the diffusion coefficient is measured without SAWs (i.e., "natural/thermal diffusion"), the pulsed laser is blocked, and additional steps are taken to further minimize the effect of room temperature fluctuations because of the need to acquire data over a very long time (e.g., 13 h to derive the longest experimental duration data point).

The data analysis follows the steps commonly used in fluorescence digital imaging microscopy [36–38,50]. The image frames taken at specific times in the experiment are processed using an algorithm that selects only the fluorescent points that fit a single Gaussian intensity profile, defined here as the point spread function of the emitter. The cluster location (i.e., XY coordinates) is obtained from the fit. The localization error is proportional to $S/\rho^{1/2}$, where S is the standard deviation of the Gaussian fit and ρ is the photon count. While a cluster-field image may contain a large number of points, only those that fit the single Gaussian fit criteria are tracked. The field of localized fluorescent emitters comprises a data set that is tracked as a function of time. The displacement [$\Delta X_i, \Delta Y_i$, and $\Delta r_i = (\Delta X_i^2 + \Delta Y_i^2)^{1/2}$] of each tracked emitter i is calculated from images taken at subsequent time intervals (Δt). The calculated displacement error is about 11 nm per axis. For the N clusters tracked, we calculate the mean $\langle \Delta r_i \rangle$ that corresponds to the collective displacement or drift in the system. The drift is then subtracted from the displacements Δr_i, and the mean square displacement (MSD) is calculated as $\text{MSD}(\Delta t) = \frac{1}{N} \sum_{i=1}^{N} (\Delta r_i - \langle \Delta r_i \rangle)^2$. A linear fit to the MSDs for several different time intervals is then used to obtain the diffusion coefficient D using the relationship $\text{MSD} = 4D\Delta t$ [50].

III. EXPERIMENTAL EVIDENCE OF THE DIFFUSION ENHANCEMENT BY SAWs

Figure 2 presents the MSD of the tracked Au$_8$ clusters plotted as a function of time for three independent experiments in which the clusters are monitored at 12 mm from the SAW source, 6 mm from the source, and with no SAW excitation. The slopes of the lines representing the best linear fits to the data points can be related to the diffusion coefficient, $D = \text{MSD}/4\Delta t$, where MSD is evaluated for the time interval
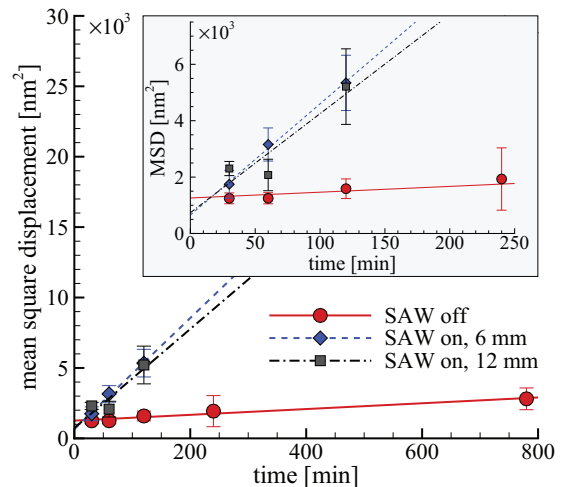

FIG. 2. (Color online) The MSD plotted as a function of time for thermally activated diffusion (no SAWs, red circles) and SAW-assisted diffusion in regions located 6 mm (blue rhombs) and 12 mm (black squares) from the SAW source. The lines are linear fits of the data sets, and the error bars show the standard error of the mean. The inset shows a magnified view for short times. The offset at zero time reflects the particle localization error inherent in optical microscopy measurements as discussed in the Supplemental Material [49].

Δt. In the absence of SAWs, the thermally mediated diffusion is characterized by $D = 8.56 \times 10^{-17}\,\text{cm}^2/\text{s}$, whereas the effective diffusion coefficients in the presence of acoustic activation are $D = 1.64 \times 10^{-15}\,\text{cm}^2/\text{s}$ at 6 mm from the source and $D = 1.46 \times 10^{-15}\,\text{cm}^2/\text{s}$ at 12 mm from the source. While, to our knowledge, there have been no prior studies of thermal diffusion of Au$_8$ on Si, the measured values of D are typical for few atom cluster species [51] and suggest that the Au$_8$ clusters do not react with the native oxide surface and retain their integrity in the course of the experiments.

Two startling conclusions arise from the experimental measurement of the diffusion coefficients. First, laser excitation of SAWs leads to a pronounced 19-fold increase in the diffusion coefficient with respect to the thermal diffusion. Second, the measured diffusion coefficient at 12 mm is nearly that as measured at 6 mm from the source, which would argue a small attenuation coefficient of the relevant SAWs. Unlike for continuous thermal activation, for SAWs the diffusion is only affected during the passage of the waves through the probe area. Given a 100 Hz laser repetition rate and a pulse duration of 6 ns, over the course of the $30-780$ min exposures used in the experiment, the acoustic source is active for mere milliseconds. This observation, combined with the relatively low frequencies of initially excited SAWs, less than 166 MHz, makes it impossible to explain the strong enhancement of surface mobility with existing physical models that only consider the effect of linear SAWs [35]. The experimental data, therefore, motivate the computational effort reported below, where nonlinear acoustic effects are fully accounted for.

IV. COMPUTATIONAL MODEL

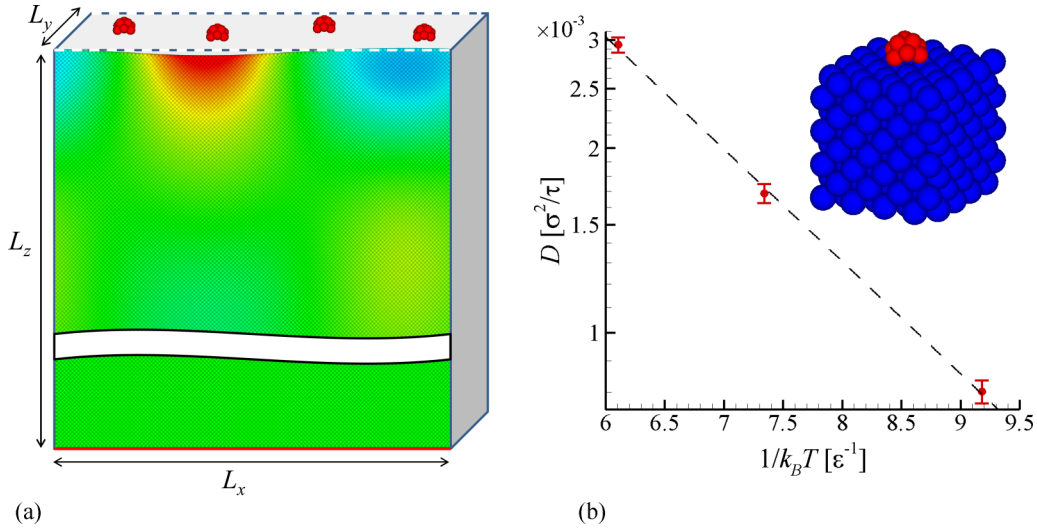In order to reveal the atomic-level mechanisms responsible for the pronounced acoustic enhancement of the surface

FIG. 3. (Color online) (a) A schematic representation of the MD computational system used in the simulations of free propagation of SAWs and (b) the Arrhenius plot of the diffusion coefficient for the thermally activated surface diffusion of a small atomic cluster in the absence of SAWs. In (a), the SAW propagates along the x direction, and the color shows an instantaneous pressure distribution for an initial sinusoidal SAW. In (b), the error bars correspond to the estimated standard error of the mean, and the fitting of the data to the Arrhenius equation yields the diffusion barrier of 0.421ε. The inset in (b) shows a fragment of the computational system with an atomic cluster (red) located on the surface of the substrate (blue).

mobility, we perform a series of large-scale molecular dynamics (MD) simulations of surface diffusion of small atomic clusters in the presence of SAWs. In contrast to earlier MD simulations of SAWs [35,52], where the close-to-sinusoidal wave profiles are generated and maintained through dynamic boundary conditions, the simulations of free nonlinear wave propagation require much larger computational systems and a careful choice of the initial and boundary conditions. These technical difficulties have prevented the application of atomistic simulations for the investigation of nonlinear SAWs so far. At the same time, the ability of MD simulations with anharmonic interatomic potentials to naturally reproduce the nonlinear sharpening of SAWs, their dissipation and interaction with surface adsorbates presents a clear advantage over continuum modeling, as the latter involves a number of assumptions and approximations [4,5,53]. A brief description of the MD model developed for the first atomistic simulations of free (nonlinear) propagation of SAWs is provided below.

A. Choice of the computational system

Given the uncertainties as to the exact structure of the cluster, its interaction with the substrate, the effect of the exposure to ambient atmosphere and presence of surface defects, as well as the length- and timescale limitations inherent to the MD simulations, we do not attempt to quantitatively mimic the experimental conditions in the simulations. Rather, we choose the parameters of the model so that the key physical features of the experimental system are reproduced. Namely, (1) on the short timescale of the MD simulations, the clusters remain motionless at the surface in the absence of SAWs, (2) the acoustic activation of cluster mobility does not lead to cluster decomposition or any significant changes in the shape of the clusters, and (3) there is no surface modification or any structural damage to the substrate under conditions of the simulations.

B. Parameters of the computational system

The system used for the MD simulations consists of a substrate with face centered cubic (fcc) structure and several clusters composed of 10 atoms each placed on the (001) surface of the substrate, as schematically shown in Fig. 3(a). The minimum distance between the clusters is chosen so that they do not have any chance to meet each other during their diffusional motion on the surface in any of the simulations. The computational system has dimensions of $L_x \times L_y \times L_z = 600 \times 5 \times 1800$ fcc unit cells and consists of 21.6 million atoms. The periodic boundary conditions are applied along x and y directions that are parallel to the free surface of the substrate, and a rigid boundary condition is applied at the bottom of the substrate.

C. Interatomic potential

The interatomic interactions in the computational system are described by the Lennard-Jones (LJ) potential with parameters σ and ε defining the length and energy scales of the substrate. A cutoff function [54] is used to ensure that the interactions vanish at a cutoff distance of 3σ. The LJ parameters for the interactions between the atoms in the clusters are $\sigma_{cc} = 0.60\sigma$ and $\varepsilon_{cc} = 3.72\varepsilon$, whereas the parameters for cluster-substrate cross-interactions are $\sigma_{cs} = \sigma$ and $\varepsilon_{cs} = 0.5\varepsilon$. The mass of an atom in a cluster is $m_c = 1.74m$, where m is the mass of an atom in the substrate. All the physical quantities obtained in the simulations are expressed in reduced units scaled by the LJ length and energy parameters, σ and ε, and atomic mass m used for the substrate.

D. Generation of SAWs

The SAWs are generated on thermally equilibrated substrates by assigning instantaneous displacements and additional velocities to all atoms in the systems according to the

analytical expressions for the continuous periodic unidirectional Rayleigh wave propagating along [100] direction on (001) surface in a cubic crystal [55]. The velocities due to the wave are added to the thermal velocities of the atoms. Following the initialization, the waves are allowed to evolve freely in dynamic simulations. The SAW propagates along the x direction, and the choice of L_x thus defines the spatial periodicity of the simulated nonlinear SAW.

The strain magnitude of the initial sinusoidal SAWs is chosen to be 0.02, which is more than 30% below the threshold for the onset of damage (plastic deformation) to the substrate. At the same time, the initial wave magnitude is sufficiently large to enable computationally efficient exploration of the effect of the acoustic activation of surface diffusion within the relatively short timescale accessible to MD simulations. In particular, the time (or distance traveled by the wave) needed for the nonlinear sharpening of the wave scales inversely with the initial strain magnitude [56], and the relatively high strength of the wave makes it possible to explore the effect of the shock front formation of the diffusion enhancement in the atomistic simulations.

E. Diffusion coefficient

The thermally and acoustically activated surface mobility of the clusters is characterized by the diffusion coefficient D calculated from the time dependence of the MSD of the cluster center of mass $4Dt = \frac{1}{N_i N_j} \sum_{i=1}^{N_i} \sum_{j=1}^{N_j} [\vec{r}_i(t + t_j) - \vec{r}_i(t_j)]^2$, where $\vec{r}_i(t)$ is the true "unfolded" (unaffected by the periodic boundary conditions) position of the center of mass of cluster i at time t, and N_i is the number of independent cluster trajectories obtained in the simulations. To collect statistically reliable information on the diffusion in the presence of SAWs, 10 simulations yielding a total of $N_i = 835$ independent trajectories of atomic clusters are performed. The duration of each simulation is 6720τ, where $\tau = (m\sigma^2/\varepsilon)^{1/2}$. Since the wave shape changes during the nonlinear propagation and dissipation, the total simulation time is divided into sixteen 420τ-long intervals, and the values of D are evaluated for each time interval.

F. Thermally activated diffusion

The diffusion barrier for thermally activated diffusion, without SAWs, is calculated to be equal to 0.421ε by performing three series of simulations at different temperatures and fitting the corresponding values of D to the Arrhenius equation, Fig. 3(b). An extrapolation of the Arrhenius dependence to a lower temperature of $0.036\varepsilon/k_B$, at which all simulations with SAWs are performed, yields $D = 3.5 \times 10^{-7}\,\sigma^2/\tau$ that corresponds to about one jump per $10^6\,\tau$. This estimation confirms that, within the simulation time of 6720τ, the probability of thermally activated jumps is virtually zero.

G. Calculation of the frequency spectrum of SAW

The spectrum of the SAW is analyzed by applying spatial fast Fourier transform (FFT) with the Hanning window function to the instantaneous displacements of the surface in the x direction caused by the SAW. The instantaneous displacements

of the substrate atoms with respect to their positions in an ideal crystal are averaged over surface subdomains with sizes of one unit cell in x direction and 4 unit cells in z direction. The pattern of the subdomain displacements obtained for one wave period is replicated to produce 2^{14} data points for the FFT. To further suppress thermal noise, the final spectrum is additionally averaged over 10 independent MD simulations, and an exponentially weighed moving average filter with an effective window size of 200τ is applied in the time domain.

V. ATOMISTIC SIMULATIONS OF THE EFFECT OF NONLINEAR SAWs ON SURFACE DIFFUSION

The mechanisms of acoustic activation of surface diffusion are investigated in a series of MD simulations of SAWs propagating on a substrate equilibrated at a temperature of $0.036\varepsilon/k_B$. In Fig. 4(a), a representative trajectory is shown for a cluster located on a substrate exposed to SAW. The cluster exhibits an active motion despite the negligible contribution of thermal diffusion expected at the temperature of $0.036\varepsilon/k_B$. Actually, the diffusion length in the acoustically activated diffusion is comparable to that of thermal diffusion but at *almost four times higher temperature*, $0.136\varepsilon/k_B$, Fig. 4(b). A notable difference between the two trajectories, however, is that the acoustically activated motion of the cluster in Fig. 4(a) starts not from the beginning of the simulation, but at a time of around 2000τ. Note that since periodic boundary conditions are applied along the direction of SAW propagation, the increasing time in the simulations corresponds to the linearly increasing distance from the source of the wave in the experiments.

The changes in the cluster mobility in the course of the nonlinear SAW propagation are revealed in Fig. 5, where the effective diffusion coefficients calculated for the 16 time intervals during the simulations are plotted. The distinct stages of the time dependence of the diffusion coefficient can be correlated with the evolution of the SAW profile illustrated in Fig. 6. During the first 1500τ, the diffusion coefficient remains below the level that can be resolved in the MD simulations while the wave profile gradually evolves from the initial sinusoidal shape generated at the beginning of the simulations, Fig. 6(a), to a shape with an increasingly steep front.

Starting from around 1500τ, the diffusion coefficient rapidly goes up (point b in Fig. 5) and reaches its peak value at around 3200τ (point c in Fig. 5). The maximum value of the diffusion coefficient is about $1.6 \times 10^{-3}\sigma^2/\tau$ that signifies more than 4500-fold increase with respect to the thermal diffusion at the substrate temperature of $0.036\varepsilon/k_B$. The temperature required to induce an equivalent diffusion by thermal activation is $0.132\varepsilon/k_B$, which is about 3.7 times higher than the actual substrate temperature maintained in the simulation. The plots of the wave profiles shown in Figs. 6(b) and 6(c) demonstrate that the onset of the cluster motion coincides with sharpening of the SAW and generation of a shock front. The pronounced cusp formed on the compressive side of the wave profile [Fig. 6(c)] is related to the nonlocal nonlinearity of SAWs [57]. The increase of the strain magnitude above the initial level in the course of the shock front formation is a distinct feature of SAWs that is
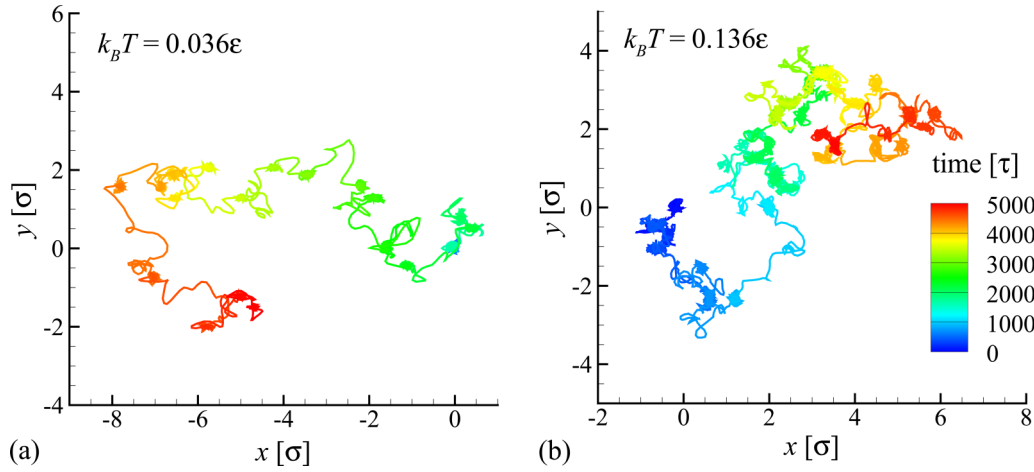
FIG. 4. (Color online) (a) The representative trajectories of the cluster center of mass recorded in simulations of SAW-induced diffusion at a temperature of $0.036\varepsilon/k_B$ and (b) thermal diffusion at a temperature of $0.136\varepsilon/k_B$. The scale is the same in both plots, the initial location of the clusters is at the origin of the coordinate system, and the trajectories are colored by time. The local displacement of the surface due to the SAW is subtracted from the instantaneous position of the cluster in (a). The temperature of 0.036ε is too low to induce any thermally activated diffusion of the cluster on the timescale of the simulation. Note that, in (a), no jumps of the cluster take place before $\sim 1500\tau$, which is the approximate time of the shock front formation. The SAW-induced cluster mobility after 2000τ is similar to that in the thermally activated diffusion at $k_B T = 0.136\varepsilon$.

not observed for bulk waves, whereas the appearance of small oscillations near the shock front is typical for a medium with dispersion.

During the next stage of the SAW profile evolution, after 3200τ, the wave amplitude and the shock front sharpness are decreasing due to the strong dissipation near the wave front,
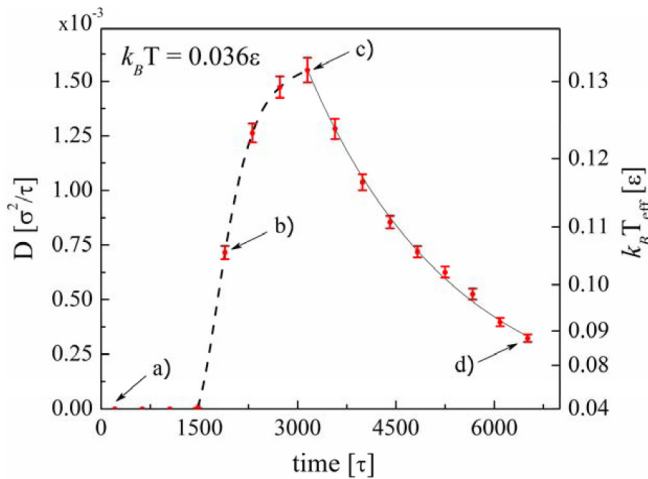

FIG. 5. (Color online) The effective diffusion coefficient at different stages of the evolution of SAW profiles. The equivalent scale of the effective temperature that would yield the corresponding diffusion coefficients by thermal activation is shown on the right side. Each data point is the result of averaging over 835 independent trajectories of atomic clusters, and the error bars show the estimated standard error of the mean. The dashed line is a guide for the eye connecting the data points for time earlier than 3200τ. The solid line is the result of an exponential fit to the data points after 3200τ (the exponential time constant is about 2400τ). The instantaneous shapes of the SAW profiles that correspond to the data points (a)–(d) labeled in the plot are shown in Fig. 6.

Fig. 6(d). The dissipation results in the exponential decrease of the cluster mobility, Fig. 5. However, despite the substantial attenuation of the wave by the time of 6500τ, the diffusion coefficient at this time still remains almost 1000 times higher than the one for thermally activated diffusion. By extrapolating the exponential decay of D beyond the time of the simulation, it can be estimated that the cluster mobility becomes comparable to the one characteristic of thermal diffusion only at around $20\,000\tau$.

To explain the connection between the SAW shock front formation and the sharp rise in the surface mobility, a detailed analysis of the cluster vibrations and the evolution of SAW spectrum are undertaken. The spectrum of thermal vibrations of the cluster on the surface reveals two main resonance peaks at about 0.13 and $0.24\tau^{-1}$ for horizontal (parallel to the surface) vibrations and higher frequencies for oscillations in the vertical direction. Therefore, harmonics with a minimum frequency of about $0.13\tau^{-1}$ must be generated for the direct resonant excitation of cluster vibrations.

The generation of high frequency harmonics in the process of SAW front sharpening can be tracked in the frequency domain by applying Fourier transform to the instantaneous displacements of the surface in x direction caused by the SAW (see Sec. IV G). The four representative spectra shown in the right frames of Fig. 6 demonstrate that the nonlinear propagation of a SAW with an initial frequency of $0.0055\tau^{-1}$ can result in dramatic changes in the spectral composition of the wave. The spectra are shown in units of the maximum acceleration for each frequency harmonic to reflect the corresponding forces acting on the adsorbed cluster. The generation of high frequency harmonics due to the wave front sharpening causes excitation forces acting at high frequencies, including the cluster resonance frequency marked by green arrow. These forces are rather strong, i.e., comparable to the force acting at the fundamental frequency of the initial wave. When the shock front is fully developed, the harmonics with frequencies
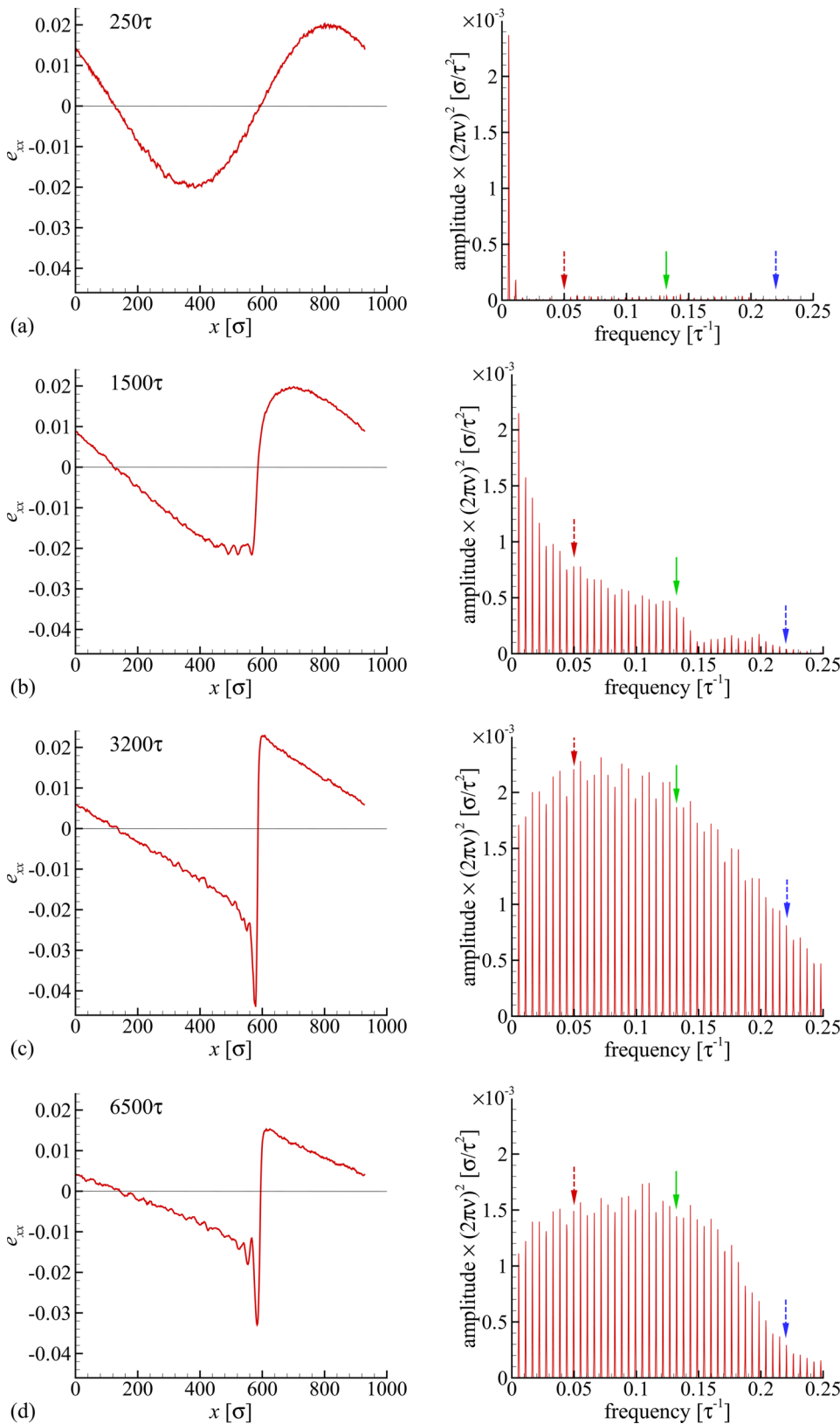
FIG. 6. (Color online) The instantaneous strain profiles (left) and the corresponding frequency spectra (right) predicted in a MD simulation of free propagation of a SAW with an initial strain amplitude of 0.02. In the frequency spectra, the maximum accelerations for different frequency harmonics are shown to illustrate the corresponding excitation forces acting on the surface adsorbates. The dashed red, solid green, and dashed blue arrows mark the harmonics with frequencies of 0.05, 0.132, and $0.22\tau^{-1}$, respectively, for which the evolution of amplitudes is shown in Fig. 7. The wave profile in (a) is close to the initial sinusoidal wave generated at the beginning of the simulation. As the SAW propagates, it exhibits sharpening of the wave profile (b) and the development of a shock front with a pronounced cusp formed at the compressive side of the wave profile (c). After the strain amplitude of the cusp reaches its maximum at $\sim 3200\tau$ (c), the magnitude of the wave starts to decrease due to the intense dissipation in the vicinity of the shock front (d).

as high as $0.5\tau^{-1}$ (corresponds to $1.4\,\text{THz}$ with the scaling discussed below) can be generated.

The three curves in Fig. 7 show the evolution of the amplitudes of three harmonics marked by arrows in both Fig. 6 and the inset of Fig. 7. The green solid line is for the harmonic that corresponds to the resonance frequency of the cluster, $0.132\tau^{-1}$, whereas the red and blue dashed lines are for the harmonics with lower and higher frequencies, 0.05 and $0.22\tau^{-1}$, respectively. It is remarkable that the amplitude of the resonance harmonic starts to rise at around 1500τ, which is
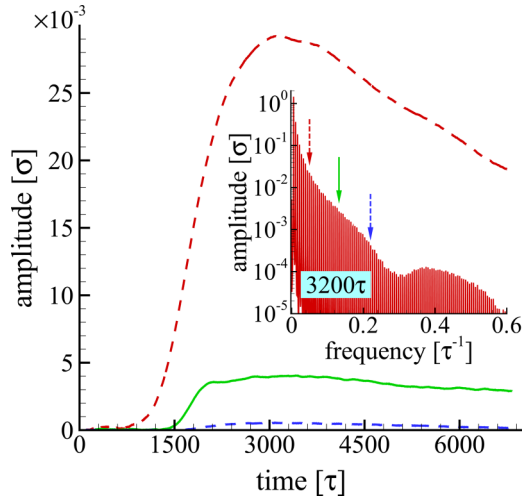
FIG. 7. (Color online) The evolution of the amplitudes of three high frequency harmonics during the nonlinear SAW propagation. The inset shows a representative frequency spectrum of a SAW for a time of 3200τ. The dashed red, solid green, and dashed blue curves correspond to harmonics with frequencies of 0.05, 0.132, and $0.22\tau^{-1}$, respectively. These frequencies are also marked by arrows in the inset and in the right panels of Fig. 6. The simulations are performed at a temperature of $0.036\varepsilon/k_B$, and the contribution of the thermal atomic vibrations to the spectrum shown in the inset is below $10^{-5}\sigma$ for all harmonics.

exactly the time when the cluster diffusion coefficient exhibits the sharp increase in Fig. 5. The amplitude of the resonant harmonic reaches its maximum value at around $3000-3200\tau$, when the cluster mobility is at its maximum. The following decrease of the amplitude correlates with the decrease of the cluster mobility after 3200τ. This direct correlation between the evolution of the high frequency components of the wave spectrum and the diffusion enhancement strongly suggests that the latter can be attributed to the dynamic coupling of high frequency harmonics with the cluster vibrational modes. The dynamic coupling has also been identified as a mechanism responsible for strong, $1-2$ orders of magnitude, enhancement of surface mobility of an individual adatom by linear (sinusoidal) SAWs at frequencies that are $3-4$ times away from the direct resonance with the adatom vibrations [35]. This observation suggests that the phenomenon of the diffusion enhancement due to the generation of high frequency harmonics in nonlinear propagation of SAWs is not specific to the diffusion of atomic clusters but is likely to be relevant to a variety of surface processes.

VI. MAPPING COMPUTATIONAL PREDICTIONS TO EXPERIMENT

The connection between the computational results and experimental observations can be established by converting the computational predictions from reduced to real physical units, using the LJ parameters of $\sigma = 3.50\,\text{Å}$, $\varepsilon = 0.534\,\text{eV}$, and $m = 56.2\,\text{Da}$. These parameters are fitted to the density of Si, $2.33\,\text{g/cm}^3$ [58], and the velocity of a Raleigh wave on {001} Si surface along $\langle 100 \rangle$ direction, $4920\,\text{m/s}$ [59], assuming that each atom in the fcc LJ crystal with a lattice parameter

of $5.43\,\text{Å}$ represents two Si atoms. The time parameter and the SAW velocity are then $\tau = (m\sigma^2/\varepsilon)^{1/2} \approx 0.366\,\text{ps}$ and $\upsilon = 5.14\,\sigma/\tau \approx 4920\,\text{m/s}$, respectively. With these parameters, the SAW generated in the simulations have the initial wavelength $\lambda = 600 \times 5.43\,\text{Å} = 326\,\text{nm}$ and frequency $\nu = \upsilon/\lambda = 15\,\text{GHz}$. During the time of a simulation, the SAW covers a distance of $6720\tau \times \upsilon = 12\,\mu\text{m}$, and the estimated maximum range of the acoustic activation of surface diffusion is $20\,000\tau \times \upsilon = 36\,\mu\text{m}$.

For the strongly nonlinear evolution of elastic waves, when the energy dissipation mostly occurs after the formation of a shock front, the characteristic time and, correspondingly, length scale of the decay of a wave increase linearly with the increasing wave period (or corresponding wavelength) [60]. Applying this reasoning for mapping the SAW dissipation observed in the simulations to the experimental conditions, the range of the acoustically affected diffusion can be expected to be on the order of 10 mm for the experimental values of $\nu \approx 10-100\,\text{MHz}$ [61] and $\lambda \approx 50-500\,\mu\text{m}$. Moreover, the inverse scaling of the shock formation distance with the initial acoustic strain [56] may further increase this range for the experimental conditions, where the strain amplitudes are likely to be much smaller than $1-2\%$ recorded for SAWs generated in Si substrates with an assistance of ablative layers [4,5,47]. Indeed, similar scaling arguments suggest that the initial strain of the order of or even smaller than 10^{-3} would be sufficient to produce the SAW front sharpening and shock front formation at the experimental length scale of several millimeters and, consequently, to yield the diffusion enhancement through the mechanism predicted in the simulations. The higher strain magnitude of the simulated waves is mainly needed to ensure that the wave front sharpening takes place at a much shorter time/length scales accessible to the atomistic simulations.

The computational prediction that the physical origin of the diffusion enhancement is the interaction of the diffusing species with the steep front of the nonlinear SAW can be used to relate the striking (more than 4500-fold) increase of the cluster diffusion coefficient in the simulations to a more moderate 19-fold increase observed in experiments. The number of wave fronts passing through the diffusion region per unit time is defined by the frequency of the continuous wave generated in the simulations, 15 GHz, and by the laser repetition rate, 100 Hz, in the experiments. The increase predicted in the simulations is from $D_{\text{th}} = 3.5 \times 10^{-7}\sigma^2/\tau$ for thermal diffusion without SAWs to $D_{\text{max}} = 1.6 \times 10^{-3}\sigma^2/\tau$ at the maximum enhancement (Fig. 5). Using the scaling to Si substrate discussed above, this increase is from $D_{\text{th}} = 1.2 \times 10^{-9}\,\text{cm}^2/\text{s}$ to $D_{\text{max}} = 5.4 \times 10^{-6}\,\text{cm}^2/\text{s}$. Since $D_{\text{th}} \ll D_{\text{max}}$, it is reasonable to assume that the thermal contribution to D_{max} is negligible and the acoustic activation is solely responsible for the high cluster mobility observed in the simulations. Scaling the value of D_{max} to the experimental repetition rate yields $D_{\text{max}} \times 100\,\text{Hz}/15\,\text{GHz} = 3.6 \times 10^{-14}\,\text{cm}^2/\text{s}$ or 22 times larger than the maximum value of the acoustically enhanced diffusion coefficient evaluated from the experimental data for 6 mm from the source, $1.64 \times 10^{-15}\,\text{cm}^2/\text{s}$. Given the approximate semiquantitative nature of the model and the lack of precise information on the strength of the SAWs generated in the experiments, the comparable orders of

magnitude of the diffusion enhancements provide an additional support for the hypothesis that the same physical mechanism of the diffusion enhancement revealed in the simulations is also responsible for the experimental observations shown in Fig. 1. Moreover, the linear scaling of the acoustically activated diffusion enhancement with the number of the SAW fronts passing the region of interest per unit time suggests that the existing sources of SAWs with frequencies on the order of tens of gigahertz [62–64] may create an equivalent of 10^3 K for surface diffusion under room temperature conditions. It is also apparent from the experimental results that an area on the order of 1 cm can be affected, thus increasing the practical use of the energy source.

VII. SUMMARY

A combined computational and experimental study of surface diffusion of small atomic clusters has revealed an enhancement of surface mobility under the action of SAWs. The direct tracking of individual gold clusters on a Si substrate by fluorescence microscopy demonstrates that the clusters can be moved by laser-generated SAWs under conditions when thermally activated diffusion is negligible. A plausible explanation of these observations is suggested based on the results of large-scale MD simulations performed for a model system that mimics the key physical characteristics of the experimental material system. The analysis of the evolution of the SAW frequency spectrum reveals a direct connection between the diffusion enhancement and the generation of high frequency harmonics associated with the nonlinear wave sharpening and shock front formation. The high harmonics reach frequencies typical of natural cluster vibrations and lead to an effective dynamic coupling between the acoustic

wave and the cluster vibrational modes. Extrapolation of the experimentally observed 19-fold diffusion enhancement from the 100 Hz pulse repetition rate to higher rates (e.g., by circularly moving the laser spot around the observation region to avoid accumulation of heat) suggests that the SAW-induced athermal increase of the diffusion coefficient by a factor of $10^2 - 10^3$ is feasible even for the experimental conditions used, although they were not specially optimized. Given the computational prediction of the key role that the nonlinear sharpening of the wave profile plays in the activation of surface diffusion, the direction of the SAW may also be optimized to ensure the strongest nonlinear effects in the wave propagation on anisotropic substrates [65].

Other surface processes, such as desorption and chemical bond rearrangements, may exhibit a similar sensitivity to the generation of high frequency harmonics in the nonlinear propagation of SAWs. The phenomenon of the acoustic activation of surface processes, therefore, can be utilized in a range of practical applications where the thermal activation should be avoided. In particular, the acoustic energy may serve as an effective substitution for heat in thin film growth on heat-sensitive substrates, cold desorption of fragile molecules for mass spectrometry analysis, or rapid switching of surface catalytic activity.

[1] K. Y. Hashimoto, *Surface Acoustic Wave Devices in Telecommunications: Modelling and Simulation* (Springer-Verlag, Berlin, Heidelberg, 2000).

[2] G. Schmera and L. B. Kish, Surface diffusion enhanced chemical sensing by surface acoustic waves, Sens. Actuators, B **93**, 159 (2003).

[3] A. Buvailo, Y. Xing, J. Hines, and E. Borguet, Thin polymer film based rapid surface acoustic wave humidity sensors, Sens. Actuators, B **156**, 444 (2011).

[4] A. Lomonosov, A. P. Mayer, and P. Hess, Laser-based surface acoustic waves in materials science, in *Modern Acoustical Techniques for the Measurement of Mechanical Properties*, edited by M. Levy, H. Bass, and R. Stern (Academic Press, San Diego, California, 2001), pp. 65–134.

[5] V. V. Kozhushko, A. M. Lomonosov, and P. Hess, Intrinsic strength of silicon crystals in pure- and combined-mode fracture without precrack, Phys. Rev. Lett. **98**, 195505 (2007).

[6] L. Y. Yeo and J. R. Friend, Surface acoustic wave microfluidics, Annu. Rev. Fluid Mech. **46**, 379 (2014).

[7] M. C. Jo and R. Guldiken, Dual surface acoustic wave-based active mixing in a microfluidic channel, Sens. Actuators, A **196**, 1 (2013).

[8] Y. Inoue, M. Matsukawa, and K. Sato, Effect of surface acoustic wave generated on ferroelectric support upon catalysis, J. Am. Chem. Soc. **111**, 8965 (1989).

[9] Y. Watanabe, Y. Inoue, and K. Sato, Activation of a thin film Pd catalyst for CO and ethanol oxidation by surface acoustic waves, Surf. Sci. **357–358**, 769 (1996).

[10] S. Kelling, T. Mitrelias, Y. Matsumoto, V. P. Ostanin, and D. A. King, Acoustic wave enhancement of the catalytic oxidation of carbon monoxide over Pt{110}, J. Chem. Phys. **107**, 5609 (1997).

[11] S. Kelling, S. Cerasari, H. H. Rotermund, G. Ertl, and D. A. King, A photoemission electron microscopy (PEEM) study of the effect of surface acoustic waves on catalytic CO oxidation over Pt{110}, Chem. Phys. Lett. **293**, 325 (1998).

[12] S. Kelling and D. A. King, Acoustic wave enhancement of catalytic reaction rates over platinum surfaces, Platinum Met. Rev. **42**, 8 (1998).

[13] H. Nishiyama, N. Rattana, N. Saito, K. Sato, and Y. Inoue, Effects of Rayleigh surface acoustic wave upon adsorptive and surface properties of a thin NiO film, J. Phys. Chem. B **104**, 10602 (2000).

[14] N. Saito, H. Nishiyama, and Y. Inoue, Acoustic wave effects on catalysis: Design of surfaces with artificially controllable functions for chemical reactions, Appl. Surf. Sci. **169–170**, 259 (2001).

[15] S. J. Reese, D. H. Hurley, and H. W. Rollins, Effect of surface acoustic waves on the catalytic decomposition of ethanol employing a comb transducer for ultrasonic generation, Ultrason. Sonochem. **13**, 283 (2006).

[16] Y. Inoue, Effects of acoustic waves-induced dynamic lattice distortion on catalytic and adsorptive properties of metal, alloy and metal oxide surfaces, Surf. Sci. Rep. **62**, 305 (2007).

[17] D. R. Denison, Phonic desorption, J. Vac. Sci. Technol. **6**, 214 (1969).

[18] C. Krischer and D. Lichtman, Observation of desorption from quartz induced by surface acoustic waves, Phys. Lett. A **44**, 99 (1973).

[19] B. Lindner and U. Seydel, Laser desorption mass spectrometry of nonvolatiles under shock wave conditions, Anal. Chem. **57**, 895 (1985).

[20] V. V. Golovlev, S. L. Allman, W. R. Garrett, and C. H. Chen, Laser-induced acoustic desorption of electrons and ions, Appl. Phys. Lett. **71**, 852 (1997).

[21] V. V. Golovlev, S. L. Allman, W. R. Garrett, N. I. Taranenko, and C. H. Chen, Laser-induced acoustic desorption, Int. J. Mass Spectrom. **169–170**, 69 (1997).

[22] A. V. Zinovev, I. V. Veryovkin, J. F. Moore, and M. J. Pellin, Laser-driven acoustic desorption of organic molecules from back-irradiated solid foils, Anal. Chem. **79**, 8232 (2007).

[23] A. M. Dow, A. R. Wittrig, and H. I. Kenttämaa, Laser-induced acoustic desorption (LIAD) mass spectrometry, Eur. J. Mass Spectrom. **18**, 77 (2012).

[24] A. J. Manzo and H. Helvajian, Demonstration of enhanced surface mobility of adsorbate cluster species by surface acoustic wave excitation induced by a pulsed laser, Proc. SPIE **8969**, 896908 (2014).

[25] F. N. Dzegilenko, T. Uzer, and E. Herbst, Classical studies of shock wave-induced desorption for model adsorbates, J. Chem. Phys. **105**, 10868 (1996).

[26] R. Almeida and E. S. Hood, Nonequilibrium dynamics in thermal desorption, J. Phys. Chem. **96**, 3086 (1992).

[27] C. Roland and G. H. Gilmer, Epitaxy on surfaces vicinal to Si(001). I. Diffusion of silicon adatoms over the terraces, Phys. Rev. B **46**, 13428 (1992).

[28] C. Ratsch, A. P. Seitsonen, and M. Scheffler, Strain dependence of surface diffusion: Ag on Ag(111) and Pt(111), Phys. Rev. B **55**, 6750 (1997).

[29] M. Mavrikakis, B. Hammer, and J. K. Nørskov, Effect of strain on the reactivity of metal surfaces, Phys. Rev. Lett. **81**, 2819 (1998).

[30] M. Schroeder and D. E. Wolf, Diffusion on strained surfaces, Surf. Sci. **375**, 129 (1997).

[31] E. Penev, P. Kratzer, and M. Scheffler, Effect of strain on surface diffusion in semiconductor heteroepitaxy, Phys. Rev. B **64**, 085401 (2001).

[32] D. J. Shu, F. Liu, and X. G. Gong, Simple generic method for predicting the effect of strain on surface diffusion, Phys. Rev. B **64**, 245410 (2001).

[33] A. van de Walle, M. Asta, and P. W. Voorhees, First-principles calculation of the effect of strain on the diffusion of Ge adatoms on Si and Ge(001) surfaces, Phys. Rev. B **67**, 041308(R) (2003).

[34] M. W. Wu and H. Metiu, The effect of strain on the adsorption of CO on Pd(100), J. Chem. Phys. **113**, 1177 (2000).

[35] C. Wu, V. Yu. Zaitsev, and L. V. Zhigilei, Acoustic enhancement of surface diffusion, J. Phys. Chem. C **117**, 9252 (2013).

[36] N. Michelotti, C. de Silva, A. E. Johnson-Buck, A. J. Manzo, and N. G. Walter, A bird's eye view: Tracking slow nanometer-scale movements of single molecular nano-assemblies, Methods Enzymol. **475**, 121 (2010).

[37] N. G. Walter, C. Y. Huang, A. J. Manzo, and M. A. Sobhy, Do-it-yourself guide: How to use the modern single-molecule toolkit, Nat. Methods **5**, 475 (2008).

[38] A. Yildiz, J. N. Forkey, S. A. McKinney, T. Ha, Y. E. Goldman, and P. R. Selvin, Myosin V walks hand-over-hand: Single fluorophore imaging with 1.5-nm localization, Science **300**, 2061 (2003).

[39] W. E. Moerner and D. P. Fromm, Methods of single-molecule fluorescence spectroscopy and microscopy, Rev. Sci. Instrum. **74**, 3597 (2003).

[40] R. Jin, S. Egusa, and N. F. Scherer, Thermally-induced formation of atomic Au clusters and conversion into nanocubes, J. Am. Chem. Soc. **126**, 9900 (2004).

[41] J. Zheng, C. Zhang, and R. M. Dickson, Highly fluorescent, water-soluble, size-tunable gold quantum dots, Phys. Rev. Lett. **93**, 077402 (2004).

[42] B. A. Collings, K. Athanassenas, D. Lacombe, D. M. Rayner, and P. A. Hackett, Optical absorption spectra of Au_7, Au_9, Au_{11}, Au_{13} and their cations: Gold clusters with 6, 7, 8, 9, 10, 11, 12, and 13 s-electrons, J. Chem. Phys. **101**, 3506 (1994).

[43] S. Lecoultre, A. Rydlo, C. Felix, J. Buttet, S. Gilb, and W. Harbich, UV-visible absorption of small gold clusters in neon: Au_n ($n = 1-5$ and 7–9), J. Chem. Phys. **134**, 074302 (2011).

[44] Y. Negishi and T. Tsukuda, Visible photoluminescence from nearly monodispersed Au_{12} clusters protected by meso-2,3-dimercaptosuccinic acid, Chem. Phys. Lett. **383**, 161 (2004).

[45] R. M. White, Generation of elastic waves by transient surface heating, J. Appl. Phys. **34**, 3559 (1963).

[46] V. E. Gusev and A. A. Karabutov, *Laser Optoacoustics* (American Institute of Physics, New York, 1993).

[47] A. Lomonosov and P. Hess, Effects of nonlinear elastic surface pulses in anisotropic silicon crystals, Phys. Rev. Lett. **83**, 3876 (1999).

[48] D. Bäuerle, *Laser Processing and Chemistry*, 3rd ed. (Springer-Verlag, Berlin, Heidelberg, 2000).

[49] See Supplemental Material at http://link.aps.org/supplemental/10.1103/PhysRevB.91.235450 for additional information on the experimental setup and data analysis.

[50] J. C. Crocker and D. G. Grier, Methods of digital video microscopy for colloidal studies, J. Colloid Interface Sci. **179**, 298 (1996).

[51] W. Xu and J. B. Adams, W dimer diffusion on W(110) and (211) surfaces, Surf. Sci. **339**, 247 (1995).

[52] C. Taillan, N. Combe, and J. Morillo, Nanoscale self-organization using standing surface acoustic waves, Phys. Rev. Lett. **106**, 076102 (2011).

[53] E. A. Zabolotskaya, Nonlinear propagation of plane and circular Rayleigh waves in isotropic solids, J. Acoust. Soc. Am. **91**, 2569 (1992).

[54] S. D. Stoddard and J. Ford, Numerical experiments on the stochastic behavior of a Lennard-Jones gas system, Phys. Rev. A **8**, 1504 (1973).

[55] R. Stoneley, The propagation of surface elastic waves in a cubic crystal, Proc. R. Soc. London A **232**, 447 (1955).

[56] E. Y. Knight, M. F. Hamilton, Y. A. Il'inskii, and E. A. Zabolotskaya, On Rayleigh wave nonlinearity, and analytical approximation of the shock formation distance, J. Acoust. Soc. Am. **102**, 2529 (1997).

[57] M. F. Hamilton, Yu. A. Il'insky, and E. A. Zabolotskaya, Local and nonlocal nonlinearity in the Rayleigh waves, J. Acoust. Soc. Am. **97**, 882 (1995).

[58] *Handbook of Chemistry and Physics*, edited by W. M. Haynes, 94th ed. (CRC Press, Boca Raton, FL, 2014).

[59] H. Coufal, K. Meyer, R. K. Grygier, P. Hess, and A. Neubrand, Precision measurement of the surface acoustic wave velocity on silicon single crystals using optical excitation and detection, J. Acoust. Soc. Am. **95**, 1158 (1994).

[60] S. N. Gurbatov, O. V. Rudenko, and A. I. Saichev, *Waves and Structures in Nonlinear Nondispersive Media* (Springer-Verlag, Berlin, Heidelberg, 2011).

[61] A. J. Manzo and H. Helvajian, Application of a laser heterodyne technique to characterize surface acoustic waves generated via a pulsed laser excitation, Proc. SPIE **8967**, 89670N (2014).

[62] M. E. Siemens, Q. Li, M. M. Murnane, H. C. Kapteyn, R. Yang, E. H. Anderson, and K. A. Nelson, High-frequency surface acoustic wave propagation in nanostructures characterized by coherent extreme ultraviolet beams, Appl. Phys. Lett. **94**, 093103 (2009).

[63] M. Schubert, M. Grossmann, O. Ristow, M. Hettich, A. Bruchhausen, E. C. S. Barretto, E. Scheer, V. Gusev, and T. Dekorsy, Spatial-temporally resolved high-frequency surface acoustic waves on silicon investigated by femtosecond spectroscopy, Appl. Phys. Lett. **101**, 013108 (2012).

[64] D. Nardi, E. Zagato, G. Ferrini, C. Giannetti, and F. Banfi, Design of a surface acoustic wave mass sensor in the 100 GHz range, Appl. Phys. Lett. **100**, 253106 (2012).

[65] A. M. Lomonosov, P. Hess, R. E. Kumon, and M. F. Hamilton, Laser-generated nonlinear surface wave pulses in silicon crystals, Phys. Rev. B **69**, 035314 (2004).